

# The Maximum Angular-Diameter Distance in Cosmology

Fulvio Melia<sup>1\*</sup> and Manoj K. Yennapureddy<sup>2†</sup>

<sup>1</sup>*Department of Physics, The Applied Math Program, and Department of Astronomy, The University of Arizona, AZ 85721, USA*

<sup>2</sup>*Department of Physics, The University of Arizona, AZ 85721, USA*

## ABSTRACT

Unlike other observational signatures in cosmology, the angular-diameter distance  $d_A(z)$  uniquely reaches a maximum (at  $z_{\max}$ ) and then shrinks to zero towards the big bang. The location of this turning point depends sensitively on the model, but has been difficult to measure. In this paper, we estimate and use  $z_{\max}$  inferred from quasar cores: (1) by employing a sample of 140 objects yielding a much reduced dispersion due to pre-constrained limits on their spectral index and luminosity, (2) by reconstructing  $d_A(z)$  using Gaussian processes, and (3) comparing the predictions of seven different cosmologies and showing that the measured value of  $z_{\max}$  can effectively discriminate between them. We find that  $z_{\max} = 1.70 \pm 0.20$ —an important new probe of the Universe’s geometry. The most strongly favoured model is  $R_h = ct$ , followed by *Planck*  $\Lambda$ CDM. Several others, including Milne, Einstein-de Sitter and Static tired light are strongly rejected. According to these results, the  $R_h = ct$  universe, which predicts  $z_{\max} = 1.718$ , has a  $\sim 92.8\%$  probability of being the correct cosmology. For consistency, we also carry out model selection based on  $d_A(z)$  itself. This test confirms that  $R_h = ct$  and *Planck*  $\Lambda$ CDM are among the few models that account for angular-size data better than those that are disfavoured by  $z_{\max}$ . The  $d_A(z)$  comparison, however, is less discerning than that with  $z_{\max}$ , due to the additional free parameter,  $H_0$ . We find that  $H_0 = 63.4 \pm 1.2 \text{ km s}^{-1} \text{ Mpc}^{-1}$  for  $R_h = ct$ , and  $69.9 \pm 1.5 \text{ km s}^{-1} \text{ Mpc}^{-1}$  for  $\Lambda$ CDM. Both are consistent with previously measured values in each model, though they differ from each other by over  $4\sigma$ . In contrast, model selection based on  $z_{\max}$  is independent of  $H_0$ .

**Key words:** cosmological parameters, cosmology: observations, cosmology: theory, distance scale, galaxies: active, quasars: supermassive black holes

## 1 INTRODUCTION

Several attempts to measure the angular diameter distance,  $d_A(z)$ , have been made over the past three decades, but so far only with limited success due to a lack of evident ‘standard rulers’ and limitations from possible size evolution with redshift. Recently, however, our understanding of compact quasar cores has improved to the point where one may now use the central, opaque regions in a luminosity-constrained sample as reliable measuring rods. These show negligible redshift evolution in the range  $0 \lesssim z \lesssim 3$ , allowing us to examine the geometry of the Universe over an even larger fraction of its age than is possible with Type Ia SNe.

Below, we will trace the history that has brought us to this point where we can meaningfully measure the redshift  $z_{\max}$  at which  $d_A(z)$  attains its maximum and use it to test various cosmological models. This is a unique aspect of the angular diameter distance, which none of the other observable signatures possess. To gauge its impact, consider that  $z_{\max} = \infty$  in a model such as the Milne universe (see, e.g., Vishwakarma 2013; Chashchina and Silagadze

2015), so one need only show that  $z_{\max}$  is finite—no matter what its actual value is—in order to rule out this cosmology.

Rather than pre-assuming a parametric form for  $d_A(z)$  based on each individual cosmology, we will employ Gaussian processes (GP; Rasmussen and Williams 2006; Holsclaw et al. 2010; Seikel et al. 2012; Yennapureddy and Melia 2017, 2018a, 2018b) to reconstruct the angular diameter distance to the compact quasar cores in a model-independent fashion. This has the dual benefit of (1) permitting us to compare the measured and predicted values of  $z_{\max}$  without any bias, and (2) to reliably measure  $z_{\max}$  even if it turns out that none of the models considered here is actually correct.

In addition, to avoid the possibility that a model may match the value of  $z_{\max}$  rather well, while still not adequately accounting for the overall reconstructed angular-diameter distance, we shall also carry out model selection based on the optimization of  $d_A(z)$  over the observed redshift range. Though related, these two diagnostics do not overlap completely. Note, e.g., that while fitting  $d_A(z)$  to the reconstructed curve requires an optimization of the Hubble constant  $H_0$ , a determination of  $z_{\max}$  is completely independent of the measured expansion rate. Thus, a consistent prioritization of the models using these two approaches will be more robust than model selection based on either of them alone. The model testing based on a

\* John Woodruff Simpson Fellow. Email: fmelia@email.arizona.edu

† manojy@email.arizona.edu

comparison of the predicted and reconstructed  $d_A(z)$  functions will be facilitated by our recent development of a differential area statistic introduced for this purpose in Yennapureddy & Melia (2018a, 2018b).

In § 2 of this paper, we will summarize the various stages of development behind the approach of measuring  $d_A(z)$ , highlighting the critical steps that have produced a sample of sources whose compact cores may be used as standard rulers. We then briefly describe in § 3 the Gaussian processes approach that will allow us to analyze these data in a cosmology independent way. The data and our method of analysis are presented in § 4, and we use the measured value of  $z_{\max}$  to compare seven different models in § 5. We will discuss the results based on the analysis of  $z_{\max}$  in § 6 and then independently carry out model selection based on how well the angular-diameter distance  $d_A(z)$  compares with the GP reconstruction over the entire redshift range in § 7. For the tests we carry out in this paper, we do not need to know the actual size of the compact structure. It will be interesting to see how its recent measurement (Cao et al. 2017b) impacts our interpretation of the Hubble constant for each model, however, and we discuss this outcome in § 8. We end with our conclusions in § 9.

## 2 BACKGROUND

An early suggestion to optimize cosmological parameters by using the angular diameter distance to compact radio sources assumed to have a fixed reference length was made by Kellermann (1993), whose analysis argued for a cosmological density close to its critical value. This claim, however, appeared to have been premature given the possible influence of source evolution with redshift. Krauss and Schramm (1993) demonstrated that the position of  $z_{\max}$  depends sensitively on the parameters, particularly the density of dark energy. They concluded that even an evolution of less than 30% in source size at  $z \lesssim 2$  could completely alter the outcome, thereby recommending that one must conclusively rule out source evolution in order to use a measurement of  $z_{\max}$  as a reliable tool for cosmology.

One possible way to mitigate the impact of source evolution is to base the standard ruler on the separation of quasar pairs (Phillipps 1994), but to establish significant constraints on the cosmological parameters one needs a sample of several hundred pairs of physically related quasars at  $z > 1$ . Even then, one needs to have an accurate assessment of the distribution of pair separations. Phillipps et al. (2002) also developed a variation on this theme, considering a proximity effect based on the observed deficit of Ly $\alpha$  forest lines at redshifts close to that of the illuminating quasar. The size of the deficient region is presumably related to the central engine's absolute luminosity. Unfortunately, this effect is difficult to disentangle from other factors, such as the intergalactic ionizing flux.

A concerted effort to better understand the evolution of radio sources and its impact on the measurement of an angular diameter distance was therefore initiated by Gurvits (1994) and Kayser (1995), who attempted to estimate how much evolution was actually occurring as a function of redshift and to what degree this affected the optimization of the model parameters. Gurvits modeled the luminosity dependence of the compact source size as  $l \sim L^\beta(1+z)^n$ , and obtained a best fit with  $\beta = 0.26 \pm 0.03$  and  $n = -0.30 \pm 0.90$ . As we shall see shortly, however, a persistent complication with compact radio sources is that they comprise a mixture of quasars, BL Lacs, OVV's, and others, so systematic dif-

ferences among them cannot be so easily disentangled from actual cosmological variations. Not surprisingly, therefore, this initial attempt was not very successful in identifying the correct cosmological model. This point was amplified by Kayser, who carefully re-analyzed the VLBI compact source data taking into account biasing of the sample from the limited resolution, and concluded at that time that a measurement of the angular diameter distance to these objects could not be used to differentiate between different models. Dabrowski et al. (1995) also pointed out that relativistic beaming cannot be ignored in such sources, since a flux-limited sample of them contains a projected-size distribution that is biased. Without a more careful identification of an appropriate sample, this approach therefore has a tendency to produce null results.

The unknown mixture of different quasar types and their possible evolution with redshift also affected the precision with which Jackson and Dodgson (1997) could use the angular diameter distance to compact cores to identify the importance of dark matter in the expansion dynamics. Nonetheless, their analysis of the angular diameter size versus redshift relation for 256 ultracompact sources with  $0.5 < z < 3.8$  did reveal a preference for a cosmology containing dark energy over one based solely on cold dark matter.

The first evidence that  $d_A(z)$  might not increase indefinitely emerged in a study of double-lobed quasars within the redshift range  $1.0 \lesssim z \lesssim 2.7$  (Buchalter et al. 1998). The apparent angular size of these objects remained more or less constant with angular-diameter distance, as one might crudely expect in most Friedmann-Robertson-Walker (FRW) cosmologies without any significant evolution (see fig. 1 below). The well-known exception is the Milne universe, for which  $d_A(z)$  increases with redshift everywhere. Similar constraints using radio galaxies as standard rulers were obtained by Podariu et al. (2003). In both cases, however, the results were weaker than those based on other kinds of observation, e.g., Type Ia SNe.

Unlike compact cores, quasars with extended jets are subject to long-term dynamical evolution and the possible influence of environment on their structure extending over galactic scales. A more specific component within the jets, i.e., shocks whose linear diameter could in principle be a standard ruler (Wiik & Valtaoja 2001), was promising, although the need to estimate their extent by monitoring their flux density and measuring light travel times, constituted a heavy reliance on the pre-assumed cosmology. The outcome was therefore compliant to the model via a somewhat circular argument. Much of the subsequent work with radio sources since that time has therefore focused on trying to reduce the scatter in the angular diameter size versus redshift relation for compact radio sources. And one of the earliest breakthroughs in this direction was made by Gurvits, Kellermann & Frey (1999), who studied 330 5 GHz VLBI contour maps (see also Frey 1999) in the redshift range  $0.011 < z < 4.72$ , demonstrating that the dispersion in this relation could be significantly reduced by restricting the sample to only those compact regions with a spectral index  $-0.38 \leq \alpha \leq 0.18$  and a total luminosity density  $Lh^2 \geq 10^{26} \text{ W Hz}^{-1}$  (with  $h$  the Hubble constant in units of  $100 \text{ km s}^{-1} \text{ Mpc}^{-1}$ ). This constraint on the spectral index still appears to be valid today and we shall use it, along with more recently developed criteria, to arrive at the sample used in this paper.

Our current view of jet launching in quasars and radio galaxies suggests that the base emission is dominated by self-absorbed synchrotron emission (Blandford & Königl 1979; Melia & Königl 1989), creating optically-thick features with angular diameters in the milliarcsecond (mas) range. At typical distances, these cores extend over roughly 10 parsecs. It is therefore likely that such small

features are influenced very little by the large-scale environment of the parent galaxies and kpc-scale jets, so their physical attributes should be similar from source to source and reasonably stable over the time they are seen (Kellermann 1993; Jackson 2004, 2008). It is thought that the morphology and kinematics of compact quasar cores are controlled by only a handful of parameters associated with the central engine itself, including its mass (and possibly the spin). Therefore, since opaque features in compact quasar cores typically last only tens of years (Gurvits, Kellermann & Frey 1999), they are expected to be free of long-term evolutionary effects in the active galactic nucleus (AGN) where they are found.

These theoretical ideas, along with the identification by Gurvits, Kellermann & Frey (1999) of a sub-sample of quasar cores with a reduced scatter in their apparent size, have generated increasing interest in using the latter as standard rulers. Lima & Alcaniz (2002) constrained the cosmic equation of state with this approach, assuming a flat FRW model driven by matter and dark energy. Like several other ensuing efforts, however, their model fits were characterized by rather large values of  $\chi^2_{\text{dof}}$  (the  $\chi^2$  per degree of freedom), indicating that the scatter in the sample was still too large to draw any definitive conclusions. In retrospect, it is not surprising that their optimized values of the model parameters are not a good match to the latest consensus (i.e., *Planck*) measurements. Similar work by Zhu & Fujimoto (2002) and Chen & Ratra (2003), using the sample of Gurvits, Kellermann & Frey (1999), attempted to constrain model parameters in cosmologies with a variable dark energy component and produced interesting limits, though weaker than those based on other methods.

An early attempt at using angular diameter distance measurements of milliarcsecond compact quasar cores to test alternative cosmological expansion scenarios was carried out by Jain, Dev & Alcaniz (2003), who simply modeled the expansion factor as a power law in time ( $a \sim t^\beta$ ), and concluded that the data at that time favoured a cosmic evolution with  $\beta = 1$ . Without the refinements we will discuss below, however, their sample had too much scatter and the errors were simply too large for them to say anything definitive about the value of  $z_{\text{max}}$ . Nonetheless, it is interesting to note that even with the inferior set of data at their disposal, their analysis seemed to indicate that a linear expansion was favoured by the observations. As we shall see later in this paper, our comparison of various cosmologies using compact quasar cores will demonstrate that the  $R_h = ct$  universe is favoured over the other models. This cosmology features a linear expansion, so our results appear to be consistent with those of Jain, Dev & Alcaniz (2003).

The sample of ultracompact radio sources often used in such studies today is that assembled by Jackson & Jannetta (2006), extracted from an old 2.29 GHz VLBI survey of Preston et al. (1985) and additions by Gurvits (1994). Their own application of these data to construct the angular diameter versus redshift diagram produced results more in line with those based on observations of the CMB, including a measurement of the angular size of the acoustic horizon. We ourselves will also use this catalog as the basis of our analysis, though with several critical improvements that we shall discuss shortly. These refinements are necessary because, as alluded to earlier, a persistent complication with ultracompact cores is that they constitute a mixed population of AGNs—quasars, BL Lacs, OVVs, etc.—making it difficult to disentangle systematic differences from true cosmological variations.

The recent introduction of an additional luminosity restriction applied to sources in the compact core sample, used in conjunction with the constraint on the spectral index  $\alpha$  used earlier by Gurvits, Kellermann & Frey (1999), appears to have overcome this weak-

ness. These authors, and independently Vishwakarma (2001), had already shown that the exclusion of sources with low luminosities  $L$  could mitigate the dependence of the intrinsic core size on  $L$  and redshift  $z$ . In their analysis of the Jackson & Jannetta (2006) sample, Cao et al. (2017a, 2017b) have demonstrated a strong dependence of the core size  $\ell_{\text{core}}$  on luminosity, not just at the low end (as had been noted earlier), but also at the high end as well (see also Cao et al. 2015; Li et al. 2016; Zheng et al. 2017). Adopting the parametrization  $\ell_{\text{core}} = \ell_0 L^\gamma (1+z)^n$ , where  $\ell_0$  is simply a scaling constant, they showed that only a sub-sample of intermediate-luminosity radio quasars in the range  $10^{27} \text{ W/Hz} < L < 10^{28} \text{ W/Hz}$  have a core size with negligible dependence on luminosity and redshift. For these sources,  $\gamma \approx 10^{-4}$  and  $|n| \approx 10^{-3}$ . Therefore, it appears that a sub-sample selected from the Jackson & Jannetta catalog with a restricted spectral index  $\alpha$  and luminosity  $L$  constitutes a compilation of compact radio cores with a reliable standard linear size.

This is the procedure we shall follow in this paper to measure  $z_{\text{max}}$  with unprecedented accuracy and to compare cosmological models in ways not previously possible using other measures of cosmological distance. In addition, we will avoid any possible biasing of the results by reconstructing the angular diameter distance of the compact cores using Gaussian processes (GP), which we now describe.

### 3 GAUSSIAN PROCESSES

Most fitting procedures require the pre-assumption of a parametric form for the fitting function tailored to the specific properties of the cosmological model. The Gaussian Processes (GP) approach (Seikel et al. 2012) avoids this shortcoming and is thereby not subject to the possibility that the predicted signature may, or may not, be a reasonable representation of the actual redshift-dependence of the measurements.<sup>1</sup>

To model a function  $f(x)$  rigorously without relying on any prior parametric form, the GP procedure assumes that the  $n$  observations of a data set  $y = \{y_1, y_2, \dots, y_n\}$  are sampled from a multivariate Gaussian distribution. The mean of the GP partnered to the data is taken to be zero. Note, however, that while modeling the data with GP is straightforward, one must face two potential areas of ambiguity with this technique. We describe these here and present steps we have developed to ensure that the outcome of the reconstruction is not affected significantly by our choice of GP components.

The first of these arises because the values of the function evaluated at different points  $x_1$  and  $x_2$  are not independent of each other. One must therefore introduce a covariance function  $k(x_1, x_2)$  to deal with the linkage between neighboring points. The difficulty is that  $k(x_1, x_2)$  is not unique or well known. There is often a broad range of such covariances. Indeed, while it makes sense to pick a function that depends only on the distance between neighboring points, this is actually not required. Most applications of this work adopt a squared exponential,

$$k(x_1, x_2) = \sigma_f^2 \exp\left(-\frac{(x_1 - x_2)^2}{2l^2}\right), \quad (1)$$

<sup>1</sup> The full details of this implementation may be found in Seikel et al. (2012), and a catalog of useful algorithms is maintained at <http://www.acgc.uct.ac.za/seikel/GAPP/index.html>

which is infinitely differentiable and useful for reconstructing both the function representing the data and its derivative.

The so-called hyperparameters  $\sigma_f$  and  $l$  are not parameters in the usual sense, since they do not specify the form of the function, but rather its ‘bumpiness.’ The length  $l$  characterizes the distance in  $x$  corresponding to a significant variation of the reconstructed function. The dependence in the ordinate direction is scaled by the signal variance  $\sigma_f$ . Equation (1) for  $\{x_1, x_2, \dots, x_n\}$  observation points leads to the covariance matrix

$$K = \begin{bmatrix} k(x_1, x_1) & k(x_1, x_2) & \dots & k(x_1, x_n) \\ k(x_2, x_1) & k(x_2, x_2) & \dots & k(x_2, x_n) \\ \dots & \dots & \dots & \dots \\ k(x_n, x_1) & k(x_n, x_2) & \dots & k(x_n, x_n) \end{bmatrix}. \quad (2)$$

The introduction of a new observation point  $x_*$  requires the evaluation of the vector

$$K_* \equiv \begin{bmatrix} k(x_*, x_1) & k(x_*, x_2) & \dots & k(x_*, x_n) \end{bmatrix}, \quad (3)$$

and the quantity  $K_{**} \equiv k(x_*, x_*)$ . Given that the data are assumed to be represented as a sample from a multivariate GP,

$$\begin{bmatrix} y \\ y_* \end{bmatrix} = N\left(0, \begin{bmatrix} K & K_*^T \\ K_* & K_{**} \end{bmatrix}\right), \quad (4)$$

the reconstruction entails the maximization of the conditional probability

$$p(y_*|y) \sim N(K_* K^{-1} y, K_{**} - K_* K^{-1} K_*^T). \quad (5)$$

This distribution has a mean  $y_*$ , which is given as

$$\mu(y_*) = K_* K^{-1} y, \quad (6)$$

with a corresponding uncertainty

$$\text{var}(y_*) = K_{**} - K_* K^{-1} K_*^T. \quad (7)$$

The reconstructed function shown in figure 1 below is based on the use of the kernel in Equation (1). To ensure that our measurement of  $z_{\text{max}}$  is not being unduly affected by this choice of covariance function, we also carry out a parallel set of simulations using a very different kind of kernel known as a Matérn covariance function, specifically the one called Matérn92 (Seikel et al. 2012), whose explicit form is

$$k(x_1, x_2) = \sigma_f^2 \exp\left(-\frac{3|x_1 - x_2|}{l}\right) \left(1 + \frac{3|x_1 - x_2|}{l} + \frac{27|x_1 - x_2|^2}{7l^2} + \frac{18|x_1 - x_2|^3}{7l^3} + \frac{27|x_1 - x_2|^4}{35l^4}\right). \quad (8)$$

In so doing, we confirm the results of previous workers, which show that the choice of kernel may change the  $p$ -values by a few points, though the outcome of model comparisons is not altered qualitatively. The rank ordering of models listed in Table 1 below is completely unaffected by the choice of covariance function.

The second potential ambiguity is associated with the hyperparameters themselves. An often used approach is to train them by maximizing the likelihood that the reconstructed function reproduces the measured values at the data points  $x_i$ . The caveat is that for a purely Bayesian analysis, the hyperparameters should be marginalized over instead of being optimized, but for our application (as is commonly the case), the marginal likelihood is sharply peaked, so optimization is a good approximation to marginalization. The bottom line is that for a set of data such as we have here (see fig. 1), there is actually no freedom to choose  $\sigma_f$  and  $l$  separately once we carry through with the optimization procedure described above.

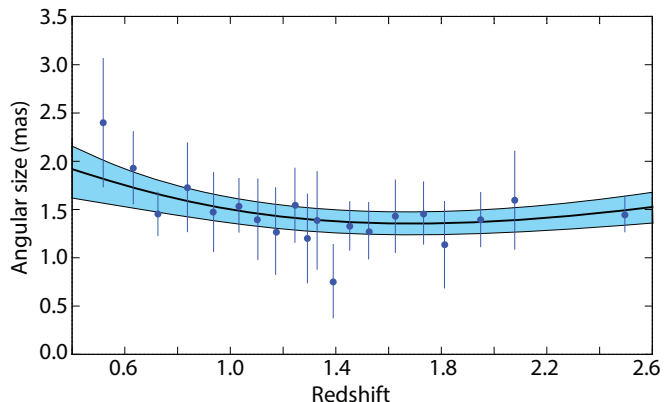


**Figure 1.** Angular size of 140 compact quasar cores divided into bins of 7, as a function of redshift. Each datum represents the median value in its bin. The thick solid curve is the reconstructed angular-size function using Gaussian processes, while the shaded region shows the  $1\sigma$  variation.

#### 4 DATA AND ANALYSIS

As we have seen from the above discussion, we may now choose from the many hundreds of available VLBI images a reduced sample of quasar cores with manageable scatter and little, if any, evolutionary effects by excluding those sources with low and high luminosities,  $L$ , and extreme spectral indices,  $\alpha$ . Specifically, the dispersion in (linear) core size  $\ell_{\text{core}}$  is significantly mitigated by selecting only sources with  $-0.38 < \alpha < 0.18$  (Gurvits, Kellermann & Frey 1999; Cao et al. 2017a, 2017b), and an intermediate-luminosity  $10^{27} \text{ W/Hz} < L < 10^{28} \text{ W/Hz}$  (Cao et al. 2017). These two criteria result in a compact quasar-core catalog with robust standard linear sizes.

The data we use here are drawn from the 613 sources assembled by Jackson & Jannetta (2006) using the 2.29 GHz VLBI survey of Preston et al. (1985) and additions by Gurvits (1994). We use the *Planck* optimized parameters (Planck Collaboration 2016) to estimate the luminosity distance which, together with the measured total flux density at 2.29 GHz, gives the luminosity  $L$ , which may be used to extract the subsample with intermediate luminosities. In doing so, we are giving *Planck*  $\Lambda$ CDM the benefit of the doubt, but note that this procedure is used merely to estimate  $L$ ; these parameters are not used in any other way during the model comparisons described below, so the results are not biased by this approach. Reducing the sample further by restricting the range of  $\alpha$  produces a final catalog of 140 sources for our analysis. We bin these sources into groups of 7 and select the median value in each bin to represent the angular size (Santos & Lima 2008). We take this step to partially minimize an additional degree of scatter that would otherwise appear using the individual data points. The resulting 20 data points are plotted in figure 1, along with their  $1\sigma$  errors estimated assuming Gaussian variation within each bin. The caveat with this approach is that the scatter may not be purely Gaussian, e.g., if there is some contribution from an unspecified systematic effect. In future work, we will address this question using a two-point diagnostic method we have already applied to other kinds of data, such as  $H(z)$  versus  $z$  (Leaf & Melia 2017a) and the HII galaxy Hubble diagram (Leaf & Melia 2017b). As we have shown in these previous applications, the two-point diagnostics very effectively indicate the quality of the errors and their likely contributions.

The angular-diameter distance (solid curve) reconstructed with Gaussian processes (GP; Rasmussen & Williams 2006;

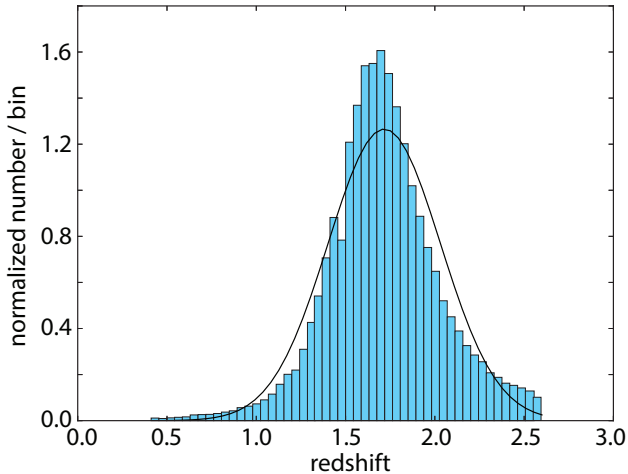


**Figure 2.** Distribution of  $z_{\max}$  values calculated from 50,000 mock samples generated from the data and errors shown in fig. 1 (see text). The histogram is truncated at  $z \sim 2.6$  due to a lack of data beyond this point. Modeling this distribution as an approximate Gaussian, we find that 68.2% of the realizations lie within a standard deviation  $\sigma_{z_{\max}} = 0.20$  of the measured value  $z_{\max} = 1.70$ .

Holsclaw et al. 2010; Seikel et al. 2012; Yennapureddy & Melia 2017, 2018a, 2018b) allows us to study the geometry of the Universe in a new, unique way. Compact radio cores have been mapped with VLBI as far out as  $z \sim 4$ , allowing us to probe the geometry of the Universe over 80% of its existence. This happens to be the redshift range within which  $d_A(z)$  first increases, reaches a maximum at some  $z_{\max}$ , and then shrinks to zero as  $z \rightarrow \infty$ . The physics behind this phenomenon is actually easy to understand (Melia 2013). The angular-diameter distance is based on the measurement of a lateral proper size, so we see the object in projection as it was when it emitted the light approaching us today. But all sources were closer to us as we look back in cosmic time, so the *apparent* angular size  $\theta_{\text{core}}$  of compact quasar cores actually increases as  $z \rightarrow \infty$ , meaning that  $d_A(z) (\sim \theta_{\text{core}}^{-1})$  therefore gets smaller.

We emphasize that as long as  $\ell_{\text{core}}$  is a true standard ruler, at least in an average sense, we do not need to know its actual value to identify  $z_{\max}$  because we are simply sampling the ratio of scales at different redshifts. We also do not need to know the Hubble constant,  $H_0$ , which does not affect the location of the turning point in  $d_A(z)$ . The net result is that the GP reconstruction shown in figure 1 is completely free of any cosmological model and assumptions. The turning point  $z_{\max}$  may then be used unambiguously to test the predictions of the models described below.

To find the error associated with this measurement of  $z_{\max}$ , we adopt the following procedure. We use the data and their  $1\sigma$  errors shown in figure 1 to create mock samples of 20 values of the core size,  $\theta_i \equiv \theta(z_i)$ , with the same redshifts,  $z_i$  ( $i = 1, \dots, 20$ ), as the actual measurements, but with Gaussian randomized values  $\theta_{\text{mock}}(z_i) = \theta(z_i) + r\sigma_i$ , where  $r$  is a Gaussian random variable with mean 0, and variance 1, and  $\sigma_i$  is the dispersion at  $z_i$ .

Then, for each mock sample, we redo the Gaussian-process reconstruction to find its corresponding  $z_{\max}$ , and repeat this process 50,000 times. The distribution of  $z_{\max}$  values thus constructed is shown as a histogram in figure 2. This distribution approximates a Gaussian, but not completely given that the data are truncated at  $z \sim 2.6$ . Its mean redshift is consistent with our measured value

$z_{\max} = 1.70$  at the maximum  $d_A$  (i.e., the minimum  $\theta_{\text{core}}$ ). Crucially, approximating this distribution as a Gaussian (shown as a solid black curve in fig. 2), we find that 68.2% of the realizations occur within a standard deviation  $\sigma_{z_{\max}} = 0.20$ , which we adopt as a reasonable estimate of the measurement error for  $z_{\max}$ .

## 5 COSMOLOGICAL MODELS

We will compare the measured value of  $z_{\max}$  with the prediction of seven different cosmological models, each with its unique expression for the angular-diameter distance,  $d_A(z)$ . As noted, the Hubble constant does not affect  $z_{\max}$ , so we do not need to specify its value.

(i) The flat *Planck*  $\Lambda$ CDM model, with parameters  $\Omega_m, \Omega_\Lambda$  and a dark-energy equation-of-state  $w_\Lambda = -1$ . In the following expressions,  $\Omega_i$  is the energy density of species  $i$ , scaled to today's critical density,  $\rho_c \equiv 3c^2 H_0^2 / 8\pi G$ . For this model,

$$d_A(z) = \frac{c}{H_0} \frac{1}{1+z} \int_0^z \frac{du}{\sqrt{\Omega_m(1+u)^3 + \Omega_\Lambda(1+u)^{3(1+w_\Lambda)}}}. \quad (9)$$

For the *Planck* parameters (Planck Collaboration 2016)  $\Omega_m = 0.308 \pm 0.012$  and  $\Omega_\Lambda = 1.0 - \Omega_m$ , we find that  $z_{\max} = 1.594$  for this model.

(ii) Einstein–de Sitter (i.e., Eq. 1 with  $\Omega_m = 1$  and  $\Omega_\Lambda = 0$ ):

$$d_A(z) = 2 \frac{c}{H_0} \frac{1}{1+z} \left( 1 - \frac{1}{\sqrt{1+z}} \right). \quad (10)$$

As with several other models introduced below, this cosmology is disfavoured by many other observations (though see Vauclair et al. 2003; Blanchard 2006), but we include it in this list because the measurement of  $z_{\max}$  provides an important complementary (and unique) measure of the Universe's geometry. The angular-diameter distance in this model attains its maximum value at  $z_{\max} = 0.682$ .

(iii) The  $R_h = ct$  Universe (a Friedmann–Robertson–Walker cosmology with zero active mass; Melia 2016a, 2017a). In this model, the total equation-of-state is  $\rho + 3p = 0$ , in terms of the energy density  $\rho$  and pressure  $p$  (Melia 2007; Melia and Shevchuk 2012). In this case,

$$d_A(z) = \frac{c}{H_0} \frac{1}{1+z} \ln(1+z), \quad (11)$$

and  $z_{\max} = 1.718$ .

(iv) The Milne Universe. This (well-known) solution is also an FRW cosmology, though with an energy density, pressure and cosmological constant all equal to zero. Its spatial curvature is negative ( $k = -1$ ). It follows from the Friedmann equations that the scale factor is linear in time (see, e.g., Vishwakarma 2013; Chashchina and Silagadze 2015). Note, however, that although it shares this linear expansion with the  $R_h = ct$  universe, the observable signatures in these two models are different because—unlike Milne—the latter is not an empty universe. In Milne, the angular-diameter distance is

$$d_A(z) = \frac{c}{H_0} \frac{1}{1+z} \sinh[\ln(1+z)], \quad (12)$$

which should be contrasted with Equation (11) for  $R_h = ct$ . Note that this expression for the angular-diameter distance has no turning point, so for Milne  $z_{\max} = \infty$ .

(v) Static Euclidean cosmology with a linear Hubble law at all redshifts:

$$d_A(z) = \frac{c}{H_0} z. \quad (13)$$

**Table 1.**  $z_{\max}$  for seven cosmological models

Model	$z_{\max}$	$ z_{\max} - z_{\max}^{\text{obs}}  / \sigma$	Probability (%)
$R_h = ct$	1.718	0.09	92.8
<i>Planck</i> $\Lambda$ CDM	1.594	0.53	59.6
Einstein-de Sitter	0.682	5.09	$\sim 0$
Milne universe	$\infty$	$\infty$	0
Static Euclidean	$\infty$	$\infty$	0
Static Euclidean tired light	$\infty$	$\infty$	0
Static Euclidean plasma tired light	$\infty$	$\infty$	0

This model, which assumes that the Universe is static, has been applied to certain specific observations (Lerner et al. 2014). The factor  $\sqrt{1+z}$  arises from the loss of energy due to a redshift without expansion. It differs from the more commonly found factor  $(1+z)$  because in this model there is no time dilation. Of course, there are significant challenges in finding consistency between this scenario and other kinds of data, but in this paper, our goal is simply to test its predicted value of  $z_{\max} = \infty$  (like Milne) against the measurement.

(vi) Static Euclidean cosmology with tired light:

$$d_A(z) = \frac{c}{H_0} \ln(1+z). \quad (14)$$

This phenomenological model assumes that photons lose energy due to some interaction along their trajectory, and that this loss of energy scales as the path length, i.e.,  $dE/dr = -(H_0/c)E$  (LaViolette 2012). Of course, as in the previous model, this ansatz is not very successful in accounting for many other observations, but our goal here again is to simply focus on the unique observational signature  $z_{\max} = \infty$  (again, like Milne).

(vii) Static Euclidean model with plasma tired light:

$$d_A(z) = \frac{c}{H_0} \ln(1+z). \quad (15)$$

In this plasma redshift application, there is an additional Compton scattering that is double that of the plasma redshift absorption (Brynjolfsson 2004; §5.8). As in Milne and the previous tired light models, we find that  $z_{\max} = \infty$ .

## 6 RESULTS BASED ON $Z_{\text{MAX}}$

Table 1 compares each model’s prediction with the measured  $z_{\max}$ , along with the difference as a fraction of  $\sigma_{z_{\max}}$  (the so-called  $z$ -value), and the corresponding probability that the predicted turning point is consistent with its measured value. Note that these percentages are absolute; in other words, we are not comparing relative probabilities, so they do not necessarily add up to one. Each individual model’s comparison with the data is independent of the relative merits of the other cosmologies.

The surprising feature of Table 1 is how strongly the various models are differentiated on the basis of  $z_{\max}$  alone, even without considering other kinds of data. One of the most important aspects of the expansion dynamics tested by Type Ia SNe is the hy-

pothesized transition from deceleration to acceleration at  $z \sim 0.7$ . Now we see that compact quasar cores play an equally important role in examining the geometry of the Universe at another critical transition redshift,  $z_{\max}$ , where the angular-diameter distance turns over. This characteristic redshift is so different between competing cosmologies that its measurement already favours only two of the models we examine here, principally  $R_h = ct$ , followed by *Planck*  $\Lambda$ CDM.

But in spite of *Planck*  $\Lambda$ CDM not being the preferred model, there is enough flexibility in the expression for  $d_A(z)$  in  $\Lambda$ CDM (Eq. 1) that we should consider whether an alternative set of parameter values might raise its standing to that of  $R_h = ct$ . Indeed, a variation of flat  $\Lambda$ CDM with  $\Omega_m = 0.23$  predicts a turning point at  $z_{\max} = 1.70$ , consistent with the measured value, and a probability exceeding 92.8%. This scaled matter density, however, would be in tension at more than  $6.5\sigma$  with the *Planck* optimized value. Additional flexibility could be introduced by relaxing the constraint that dark energy is a cosmological constant, so that  $w_{\text{de}} \neq -1$ . But with each such modification to the standard model, we recede further and further from the concordance *Planck* cosmology, calling into question whether finding consistency with the measured value of  $z_{\max}$  is worth damaging the optimization of fits to other data, including the cosmic microwave background.

Aside from this head-to-head comparison between  $R_h = ct$  and  $\Lambda$ CDM, the results in Table 1 also strongly support other observations that have disfavoured—or even rejected—the other five models examined here. For example, note how different the outcome is for Milne compared to  $R_h = ct$ . Given that both of these models predict a linear expansion rate, they are still sometimes confused with each other in the literature. On occasion, Milne is compared to  $\Lambda$ CDM to ‘demonstrate’ that  $R_h = ct$  is disfavoured by the data (see, e.g., Melia 2015, and references cited therein). But as is clearly demonstrated here, the observational signatures associated with Milne are very different from those in  $R_h = ct$  and, while the latter is favoured by the data, the former is strongly ruled out.

Finally, we comment on one of the issues highlighted in § 3 concerning a possible influence due to the choice of covariance function  $k(x_1, x_2)$  while using Gaussian processes. As we alluded to earlier, the choice of  $k$  in Equation (1) is not unique, though this particular function has found widespread appeal with GP applications (see, e.g., Rasmussen & Williams 2006; Holsclaw et al. 2010; Seikel et al. 2012; Yennapureddy & Melia 2017, 2018a, 2018b). What determines whether or not a particular function is appropriate is how far the correlation extends to either side of each datum, and

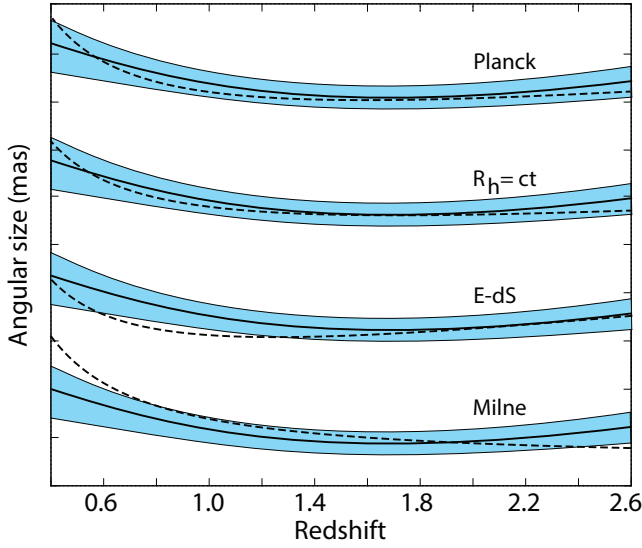


**Figure 3.** Comparison of the GP reconstructed quasar core size  $\theta_{\text{core}}(z)$  (solid curve, from fig. 1) with the model prediction (dashed) for the *Planck*  $\Lambda$ CDM,  $R_h = ct$ , Einstein-de Sitter and Milne cosmologies. The four plots have been staggered vertically for clarity. In each case, the shaded swath represents the  $1\sigma$  confidence region for the reconstruction (see fig. 1). The cumulative distribution is shown in fig. 5, and the values of  $\eta$  (Eq. 17) for the optimized fits, along with the corresponding probabilities, are listed in Table 2.

whether the chosen  $k$  adequately models this correlation in terms of the hyperparameter  $l$  (and to a lesser degree  $\sigma_f$ ). We have therefore tested the correlation in our data set by reconstructing the angular size function in figure 1 using the very different kernel in Equation (8). The results are virtually identical to those shown in Table 1, except that the individual percentages change by a few points or less. Very importantly, the rank ordering of these seven models remains exactly the same as that shown here. We are therefore confident that the GP method has been applied correctly to these data.

## 7 RESULTS BASED ON $D_A(Z)$

One of the strengths of the  $z_{\text{max}}$  diagnostic is that its determination is completely independent of the Hubble constant  $H_0$ . Thus all models may be compared with each other on level ground. But as we alluded to above, there is always the possibility that a model’s prediction may match the turning point rather well, while its angular-diameter distance  $d_A(z)$  is overall a poor match to the GP reconstructed curve in figure 1. To compare the predicted and measured  $d_A(z)$  functions, however, it is necessary to optimize the vertical scaling (proportional to  $c/H_0$ ) in equations (9-15) individually for each cosmology. We do this by writing the theoretical angular size of the compact quasar core as

$$\theta_{\text{core}}^{\text{th}}(z) = \frac{\ell_{\text{core}}}{d_A(z)}, \quad (16)$$

where  $\ell_{\text{core}}$  is the physical core size, assumed to be more or less constant from source to source in the reduced quasar sample. To carry out the analysis in this paper, we do not need to know the actual value of  $\ell_{\text{core}}$  and  $H_0$ , and we may combine them by merging the expression for  $\theta_{\text{core}}(z)$  and  $d_A(z)$  for each model, writing

$$\theta_{\text{core}}^{\text{th}}(z) = \frac{\eta}{\mathcal{I}(z)}, \quad (17)$$

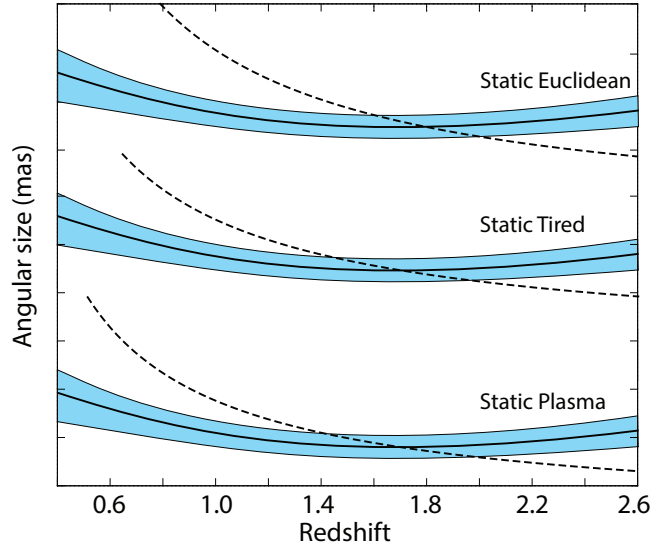


**Figure 4.** Same as fig. 3, except now for the Static Euclidean, Static Tired Light and Static Plasma Tired Light cosmologies. As indicated in fig. 5 and Table 2, these three models are disfavoured by the data in comparison with the *Planck* and  $R_h = ct$  models.

where  $\eta \equiv \ell_{\text{core}}H_0/c$  and

$$\mathcal{I}(z) \equiv \left(\frac{H_0}{c}\right)d_A(z). \quad (18)$$

As we shall see shortly, however, a recent measurement of  $\ell_{\text{core}}$  by Cao et al. (2017b) allows us to see what the optimized value of  $\eta$  implies for the Hubble constant in each cosmology. In order to cast each model in its best possible light, we optimize the parameter  $\eta$  individually in each case to yield the best match with the GP reconstructed curve, following a procedure described in Yennapureddy & Melia (2018a, 2018b), and briefly summarized below.

The best fit curves for the models we test in this paper are shown in comparison with the GP reconstruction and its confidence region (shaded swath) in figs. 3 and 4. Even a quick inspection by eye shows that Einstein-de Sitter, Milne, and especially Static Euclidean, Static Tired Light and Static Plasma, extend beyond the  $1\sigma$  region and are therefore not well matched to the data. *Planck* and  $R_h = ct$  do much better, as reflected also in the probabilities displayed in Table 2.

When comparing two continuous functions, i.e., the reconstructed  $\theta_{\text{core}}(z)$  curve in figure 1 with  $\theta_{\text{core}}^{\text{th}}(z)$  in Equation (17), one may not use discrete sampling statistics because sampling at random points to obtain the differences between the two curves would lose information, whose importance is difficult to ascertain. We have recently introduced a new diagnostic, called the “Area Minimization Statistic,” to estimate the probability that a model is consistent with the data. Assuming that the measurement errors are Gaussian, one generates a mock sample of GP reconstructed curves covering the likely variation of  $\theta_{\text{core}}(z)$  away from the function representing the actual data. This is done by using the Gaussian randomization

$$\theta_{\text{core}}^{\text{mock},i}(z) = \theta_{\text{core}}^i(z) + r\sigma_{\theta_{\text{core}}^i}, \quad (19)$$

where  $\theta_{\text{core}}^i(z)$  are the actual measurements and  $\sigma_{\theta_{\text{core}}^i}$  are the corresponding errors. Also,  $r$  is a Gaussian random variable with zero mean and a variance of 1. GP are then used with these  $\theta_{\text{core}}^{\text{mock},i}(z)$  mock data and their errors  $\sigma_{\theta_{\text{core}}^i}$  to reconstruct the function  $\theta_{\text{core}}^{\text{mock}}(z)$

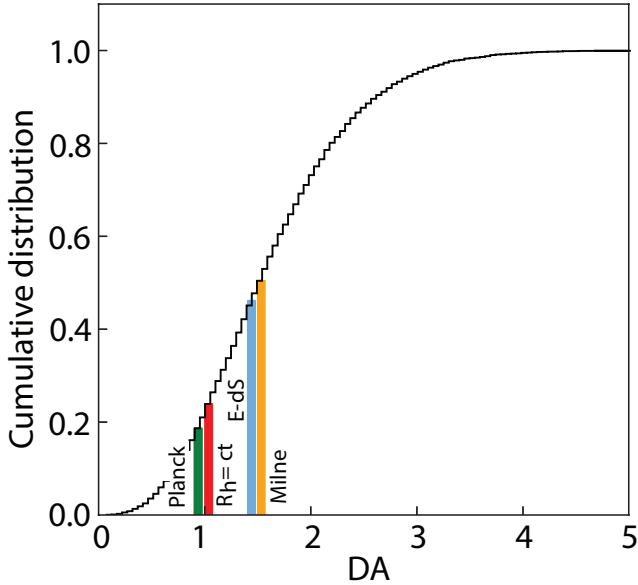


**Figure 5.** Cumulative probability distribution for the area differential  $DA$  (Eqn. 20), and the estimated values for the cosmological models considered in this paper. The two cosmologies favoured by this test are *Planck* and  $R_h = ct$ , all with a probability  $\sim 0.8$ , as indicated in Table 2. The other 3 (static) models are off the chart to the right, consistent with zero probability (see Table 2).

representing each mock sample. In the final step, we determine the weighted absolute area difference

$$DA = \int_{z_{\min}}^{z_{\max}} dz \frac{|\theta_{\text{core}}^{\text{mock}}(z) - \theta_{\text{core}}(z)|}{\sigma_{\text{GP}}(z)}. \quad (20)$$

Here,  $z_{\min}$  and  $z_{\max}$  are the minimum and maximum redshifts, respectively, of the data range, and  $\sigma_{\text{GP}}(z)$  is the calculated dispersion (corresponding to the shaded region in fig. 1) associated with the GP reconstructed curve  $\theta_{\text{core}}(z)$ . Repeating this procedure 10,000 times, we build the probability distribution for the area differential  $DA$ , which is shown in fig. 5, along with the individually measured values of  $DA$  for each model we test. With the assumption that a smaller  $DA$  corresponds to a better match to  $\theta_{\text{core}}(z)$ , the cumulative distribution may then be used to estimate the likelihood that the difference between a model’s prediction and  $\theta_{\text{core}}(z)$  is due principally to Gaussian randomness, rather than the model being wrong. A comparison of the likelihoods then prioritizes the models according to their probability of matching the data. Many statistical approaches utilize this basic concept, but unfortunately none of the existing methods may be used for the comparison of two continuous curves, as we have here.

The model selection based on the angular-diameter distance supports the outcome of the  $z_{\max}$  diagnostic. The two models favoured by a comparison of the reconstructed and predicted  $d_A(z)$  functions, i.e., *Planck*  $\Lambda$ CDM and  $R_h = ct$ , are also those most strongly selected according to how well they account for the observed turning point in  $d_A(z)$ . But while *Planck*  $\Lambda$ CDM and  $R_h = ct$  are virtually indistinguishable from each other in fig. 5 and Table 2, their prioritization based on  $z_{\max}$  is much stronger (see Table 1). This is largely due to the fact that, while  $\ell_{\text{core}}$  and  $H_0$  are not used in the identification of the turning point  $z_{\max}$ , one needs to opti-

mize the ratio of these two unknowns in order to find the best fit for  $d_A(z)$ . This freedom to optimize  $\eta$  makes it easier for a model to fit the angular-size data, so the differences between the two favoured models are somewhat mitigated. This is the principal reason we highlighted the  $z_{\max}$  diagnostic as being superior to  $d_A(z)$  for model selection, given that it requires no optimization of free parameters, allowing all of the models to be compared on level ground.

## 8 DISCUSSION

We have emphasized throughout this paper that knowing the actual value of  $\ell_{\text{core}}$  and  $H_0$  is not necessary to conduct the model comparisons based on the quasar compact core data. Attempts at measuring  $\ell_{\text{core}}$  have already met with some success (Cao et al. 2017b), however, so it would be interesting to see what impact this result ( $\ell_{\text{core}} = 11.03 \pm 0.25$  pc) has on the implied value of the Hubble constant  $H_0$  via the optimized  $\eta$  in Table 2. From the definition of  $\eta$  (near Eq. 18), we infer that  $H_0 = 63.4 \pm 1.2$  km s<sup>-1</sup> Mpc<sup>-1</sup> in the case of  $R_h = ct$ , and  $H_0 = 69.9 \pm 1.5$  km s<sup>-1</sup> Mpc<sup>-1</sup> for  $\Lambda$ CDM. Both of these are completely consistent with previously measured values of the Hubble constant in each cosmology. The confirmation is provided by the latest *Planck* release (Planck Collaboration 2016), and the four previous measurements reported for  $R_h = ct$ :  $63.2 \pm 1.6$  km s<sup>-1</sup> Mpc<sup>-1</sup> (Melia & Maier 2013);  $63.3 \pm 7.7$  km s<sup>-1</sup> Mpc<sup>-1</sup> (Melia & McClintock 2015);  $62.3^{+1.5}_{-1.4}$  km s<sup>-1</sup> Mpc<sup>-1</sup> (Wei, Melia & Wu 2017); and  $63.0 \pm 1.2$  km s<sup>-1</sup> Mpc<sup>-1</sup> (Melia & Yennapureddy 2018).

Aside from actually obtaining a value for  $\ell_{\text{core}}$ , Cao et al. (2017b) showed through their analysis, based on measurements of  $H(z)$  using cosmic chronometers, that this length scale is independent of redshift, making it a true standard ruler. As long as these measurements are fully model-independent and free of any systematic effects, the use of compact structure in quasar cores with this  $\ell_{\text{core}}$  may constitute a powerful diagnostic for cosmological measurements, such as  $H_0$ . Already, we have found complete consistency between this approach and previous measurements, including the *Planck* optimization of model parameters.

It should also be remarked that in both cases (i.e.,  $R_h = ct$  and  $\Lambda$ CDM), the inferred value of  $H_0$  disagrees with the local measurement based on Cepheid variables (Riess et al. 2018). It is not yet clear why this happens, but some authors have speculated on the possibility that a local ‘Hubble Bubble’ (Shi 1997; Keenan et al. 2013; Romano 2017; Wei et al. 2017) may be influencing the dynamics within a distance  $\sim 300$  Mpc (i.e.,  $z < 0.07$ ). If true, such a fluctuation might lead to anomalous velocities within this region, causing the nearby expansion to deviate somewhat from a pure Hubble flow. Until this issue is resolved, we must rely on the large-scale measurement of  $H_0$  individually for each model.

## 9 CONCLUSION

Our ability to measure  $z_{\max}$  has created an entirely new probe of the Universe’s geometry. In this paper, we have shown that the predicted value of this turning point changes considerably between different models, allowing existing measurements, e.g., of compact quasar-core sizes, to disfavour all but two of the models we examined. The model preferred by these data is  $R_h = ct$ , which also happens to be the cosmology with the fewest parameters. Indeed, for the purpose of comparing values of  $z_{\max}$ , this cosmology has no



**Table 2.** DA statistics for seven cosmological models

Model	$\eta$	Probability (%)
<i>Planck</i> $\Lambda$ CDM	0.53	81
$R_h = ct$	0.48	76
Einstein-de Sitter	0.19	52
Milne universe	0.57	50
Static Euclidean	2.23	0
Static Euclidean tired light	1.31	0
Static Euclidean plasma tired light	1.31	0

parameters at all, which makes the consistency between its prediction ( $z_{\max}^{R_h=ct} = 1.718$ ) and the measured value ( $z_{\max} = 1.70 \pm 0.20$ ) quite compelling. *Planck*  $\Lambda$ CDM is not yet ruled out by these observations, but in order to bring its prediction in line with the observations, one must adopt a scaled matter density  $\Omega_m = 0.23$  in tension with *Planck* at over  $6.5\sigma$ .

We have highlighted the measurement of  $z_{\max}$  as the most probative diagnostic for model selection based on angular sizes, principally because it relies on fewer parameters than the angular-diameter distance itself. But to ensure that the predicted  $d_A(z)$  is consistent with the GP reconstructed function for the preferred models, we have also compared the overall angular-diameter distance to the data. The two models most highly favoured by this comparison, *Planck*  $\Lambda$ CDM and  $R_h = ct$ , are also those most strongly preferred by  $z_{\max}$ . But unlike the latter, a comparison of  $d_A(z)$  with the data is less discerning for these two models, mainly due to the additional free parameter,  $H_0$ , which provides more flexibility with the best fit. For example, the optimized value of  $H_0$  is  $63.4 \pm 1.2 \text{ km s}^{-1} \text{ Mpc}^{-1}$  for  $R_h = ct$ , and  $69.9 \pm 1.5 \text{ km s}^{-1} \text{ Mpc}^{-1}$  for  $\Lambda$ CDM. Both are fully consistent with previously measured values of the Hubble constant in each model, though they differ from each other at about  $4\sigma$ . In contrast, model selection based on  $z_{\max}$  is independent of  $H_0$ .

All of the comparative tests completed thus far (see, e.g., Table 1 in Melia 2017b for a summary and references) suggest that the zero active mass condition in general relativity is the influence guiding the Universe's expansion. Several exciting new tests are under development, including the measurement of redshift drift (Melia 2016b) and the detection of progenitors to high- $z$  quasars (Fatuzzo & Melia 2017). Within a few years, we should know for certain whether or not  $R_h = ct$  is the correct cosmology. The consequences are far reaching. Chief among them is the fact that, while inflation is necessary to maintain the internal self-consistency of  $\Lambda$ CDM, it is not required for (and is actually inconsistent with) the zero active mass condition (Melia 2014).

#### ACKNOWLEDGMENTS

We are grateful to the anonymous referee and Louis Marmet for providing a helpful set of comments and suggestions that have led to a significant improvement in this manuscript. FM is also grateful to Amherst College for its support through a John Woodruff Simpson Lectureship, and to Purple Mountain Observatory in Nanjing,

China, for its hospitality while part of this work was being carried out. This work was partially supported by grant 2012T1J0011 from The Chinese Academy of Sciences Visiting Professorships for Senior International Scientists, and grant GDJ20120491013 from the Chinese State Administration of Foreign Experts Affairs.

#### REFERENCES

- Blanchard, A., 2006, in: Current issues in Cosmology, eds. J.-C. Pecker and J. V. Narlikar, (Cambridge University Press, Cambridge U.K., p. 76
- Blandford, R. D. & Königl, A., 1979, *ApJ*, 232, 34
- Brynjolfsson, A., 2004, arXiv:astro-ph/0401420
- Buchalter, A. et al., 1998, *ApJ*, 494, 503
- Cao, S. et al., 2015, *ApJ*, 806, 66
- Cao, S. et al., 2017a, *JCAP*, 02, id. 012
- Cao, S. et al., 2017b, *A&A*, 606, A15
- Chashchina, O. I. and Silagadze, Z. K., 2015, *Universe*, 1, 307
- Chen, G. & Ratra, B., 2003, *ApJ*, 582, 586
- Dabrowski, Y., Lasenby, A. and Saunders, R., 1995, *MNRAS*, 277, 753
- Fatuzzo, M. & Melia, F., 2017, *ApJ*, 846, 129
- Frey, S., 1999, *New Astronomy Reviews*, 43, 761
- Gurvits, L. I., 1994, *ApJ*, 425, 442
- Gurvits, L. I., Kellermann, K. I. & Frey, S., 1999, *A&A*, 342, 378
- Holsclaw, T., Alam, U., Sanso, B., Lee, H., Heitmann, K., Habib, S. & Higdon, D., 2010, *PRL*, 105, id. 241302
- Jackson, J. C., 2004, *JCAP*, 11, id. 007
- Jackson, J. C., 2008, *MNRAS*, 390, L1
- Jackson, J. C. and Dodgson, M., 1997, *MNRAS*, 285, 806
- Jackson, J. C. & Jannetta, A. L., 2006, *JCAP*, 11, 002
- Jain, D., Dev, A. & Alcaniz, J. S., 2003, *CQG*, 20, 4485
- Kayser, R., 1995, *A&A*, 294L, L21
- Keenan, R. C., Barger, A. J., Cowie, L. L., 2013, *ApJ*, 775, 62
- Kellermann K. I., 1993, *Nature*, 361, 134
- Krauss, L. M. and Schramm, D. N., 1993, *ApJ Letters*, 405, L43
- LaViolette, P. A., 2012, *Subquantum kinetics: The Alchemy of Creation*, 4th ed. (Starlane Pub., Niskayana NY)
- Leaf, K. & Melia, F., 2017a, *MNRAS*, 470, 2320
- Leaf, K. & Melia, F., 2017b, *MNRAS*, 474, 4507
- Lerner, E. J., Falomo, R. and Scarpa, R., 2014, *IJMP-D*, 23, id. 1450058
- Li, X.-L. et al., 2016, *RAA*, 16, 84

- Lima, J.A.S. & Alcaniz, J. S., 2002, ApJ, 566, 15  
Melia, F., 2007, MNRAS, 382, 1917  
Melia, F., 2013, CQG, 30, 155007  
Melia, F., 2014, A&A, 561, id. A80  
Melia, F., 2015, MNRAS, 446, 1191  
Melia, F., 2016a, Front. Phys., 11, 119801  
Melia, F., 2016b, MNRAS Letters, 463, L61  
Melia, F., 2017a, Front. Phys., 12, 129802  
Melia, F., 2017b, MNRAS, 464, 1966  
Melia, F. & Königl, A., 1989, ApJ, 340, 162  
Melia, F. & Maier, R. S., 2013, MNRAS, 432, 2669  
Melia, F. & McClintock, T. M., 2015, AJ, 150, 119  
Melia, F. & Shevchuk, A., 2012, MNRAS, 419, 2579  
Melia, F. & Yennapureddy, M. K., 2018, JCAP, 02, 034  
Phillipps, S., 1994, MNRAS, 269, 1077  
Phillipps, S., Horleston, N. J. and White, A. C., 2002, MNRAS, 336, 587  
Planck Collaboration et al., 2016, A&A, 594, id A13  
Podariu, S., Daly, R. A., Mory, M. P. & Ratra, B., 2003, ApJ, 584, 577  
Preston, R. A., 1985, AJ, 90, 1599  
Rasmussen, C. & Williams, C., 2006, Gaussian Processes for Machine Learning (The MIT Press, Cambridge)  
Riess, A. G. et al., 2018, e-print (arXiv:1804.10655)  
Romano, A. E., 2017, e-print (arXiv:1609.04081)  
Santos, R. C. & Lima, J.A.S., 2008, PRD, 77, 083505  
Seikel, M., Clarkson, C. & Smith, M., 2012, JCAP, 06, 036S  
Shi X., 1997, ApJ, 486, 32  
Vauclair, S. C. et al., 2003, A&A, 412, L37  
Vishwakarma, R. G., 2001, CQG, 18, 1159  
Vishwakarma, R. G., 2013, Phys. Scr., 87, 055901  
Wei, J.-J., Melia, F. & Wu, X., 2017, ApJ, 835, 270  
Wiik, K. and Valtaoja, E., 2001, A&A, 366, 1061  
Yennapureddy, M. K. & Melia, F., 2017, JCAP, 11, 029 (arXiv:1711.03454)  
Yennapureddy, M. K. & Melia, F., 2018a, EPJ-C, 78, 258  
Yennapureddy, M. K. & Melia, F., 2018b, JCAP, 02, 034 (arXiv:1802.02255)  
Zheng, X. et al., 2017, JCAP, 10, 030  
Zhu, Z.-H. & Fujimoto, M. K., 2002, ApJ, 581,1